Chapter 15

Ultrafast Carrier Dynamics at p-n Junction of Cu(In,Ga)Se_2-Based Solar Cells Measured by Optical Pump Terahertz Probe Spectroscopy

Woo-Jung Lee and Yong-Duck Chung

Additional information is available at the end of the chapter

http://dx.doi.org/10.5772/66350

Abstract

Among other materials, the p-type Cu(In,Ga)Se_2 (CIGS) alloy has attracted attention as the most efficient absorber in thin-film solar cells. The typical CIGS layer is deposited with a polycrystalline structure containing an amount of native defect states, which serve as carrier traps and recombination centers. These defect states in the CIGS layer can be easily changed after deposition of an n-type buffer layer, due to the formation of p-n junctions. To understand the influence of the p-n junction on these defect states, the behavior of photoexcited carriers, from the CIGS absorber to the buffer layer, is considered to be an important issue and is closely related to solar cell performance. In this study, we performed experiments to investigate the ultrafast carrier dynamics of CIGS-based solar cells, using optical pump terahertz (THz) probe (OPTP) spectroscopy, and demonstrated the correlation between solar cell performance and the behavior of photoexcited carrier dynamics.

Keywords: ultrafast carrier dynamics, Cu(In,Ga)Se_2, optical pump terahertz probe spectroscopy, p-n junction, defect states

1. Introduction

1.1. Basic properties of a CIGS solar cell

Cu(In,Ga)Se_2 (CIGS) is an attractive material for solar cells because of its beneficial qualities, including a high absorption coefficient for visible light, favorable direct bandgap (Eg), and great power conversion efficiency [1–5]. CIGS is comprised of $CuInSe_2$ (CIS)-$CuGaSe_2$ (CGS) and its *Eg* can be controlled from 1.04 eV of CIS to 1.68 eV of CGS by adding Ga content into the CIS. A CIGS of a ternary compound consists of a group I element (Cu), III elements

INTECH
open science | open minds

© 2017 The Author(s). Licensee InTech. This chapter is distributed under the terms of the Creative Commons Attribution License (http://creativecommons.org/licenses/by/3.0), which permits unrestricted use, distribution, and reproduction in any medium, provided the original work is properly cited. CC BY

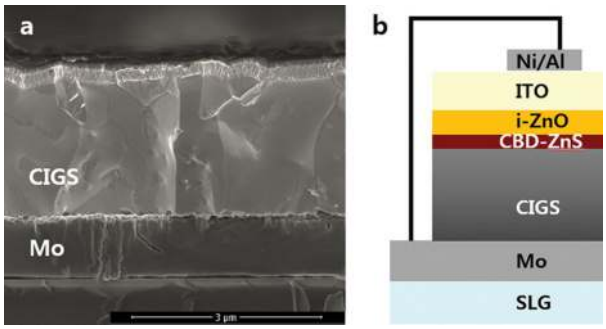

Figure 1. (a) The cross-section image of a CIGS solar cell with a CBD-ZnS buffer layer obtained by scanning electron microscopy and (b) the schematic diagram of a completed CIGS solar cell structure.

(Ga, In), and IV elements (Se), which are tetrahedrally bonded with a chalcopyrite crystal structure. The CIGS is generally deposited as a polycrystalline structure with an amount of native defect states and grain boundaries, which serve as carrier traps and recombination centers [6–8]. Representatively, there are 12 intrinsic defect states in CIGS: 3 vacancies (V_I, V_{III}, and V_{VI}), 3 interstitials (I_i, III_i, and VI_i), and 6 antisite defects (I_{III}, I_{VI}, III_I, III_{VI}, V_I, and VI_{III}). These defect states can work as either acceptors or donors by enthalpy of formation energy. The typical CIGS is considered to be a p-type material because of the amount of negatively charged Cu vacancies (V_{Cu}) with acceptor characteristics [9].

A CIGS solar cell with a chemical bath deposited-ZnS (CBD-ZnS) buffer layer is composed of several stacked layers, as indicated in the scanning electron microscopy (SEM) image of **Figure 1a**. p-Type CIGS layers with a polycrystalline structure approximately 2.2 μm thick were deposited by the conventional coevaporation method of a multistage process on Mo coated soda lime glass (SLG) [10–12]. As the n-type buffer layer, CBD-ZnS with a thickness of ~30 nm was prepared on the CIGS layer by precipitation from an aqueous solution. RF sputtering was then conducted to form an i-ZnO(70 nm)/ITO(150 nm) film as the transparent conducting oxide (TCO) layer. Finally, a current-collecting grid of Ni(50 nm)/Al(3 μm) was deposited by e-beam evaporation, completing the structure of the solar cell described in **Figure 1b**.

In CIGS-based solar cells, understanding the interfacial reaction at the p-n junction between the p-type CIGS absorber and n-type buffer layer is particularly important. This is because the intrinsic defect states in the CIGS, which experience a metastable redistribution of charge carriers after deposition of the buffer layer, have an influence on device performance [13–15]. Moreover, these defect states and the properties of the p-n junction have a decisive effect on the carrier relaxation dynamics in the CIGS layer, dominating the device performance. Thus, to improve the CIGS efficiency in a solar cell, it is essential to understand the intrinsic characteristics of the native defects in the CIGS, and the p-n junction.

http://dx.doi.org/10.5772/66350

1.2. Optical pump-THz probe spectroscopy

Among various measurement tools, optical pump terahertz (THz) probe (OPTP) spectroscopy was utilized in this experiment to verify the effect of the defect states because it is an extremely sensitive tool for investigating scattering mechanisms and dynamic energy transitions of photoexcited carriers in the region of shorter timescales on the order of ~*f*s and *p*s [16–18]. **Figure 2** shows the equipment system of the OPTP spectroscopy used in this study [19]. The detailed explanation for ingredients of the system is described as follows.

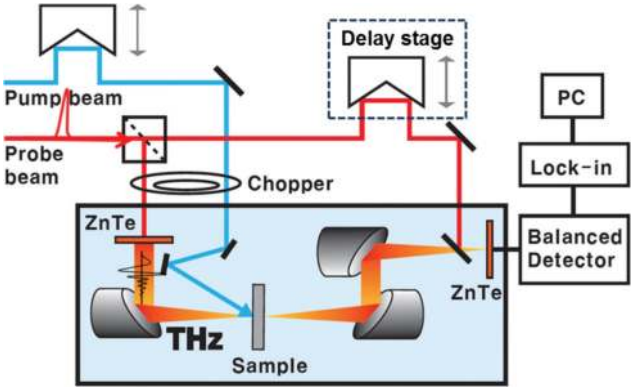

Figure 2. Schematic diagram of OPTP measurement system.

To measure the photoexcited carrier dynamics related with defect states, THz-time domain spectroscopy (in short, THz-TDs) measurement is carried out in advance. A fs pulse laser with 800 nm wavelength and pulse duration of 120 fs is generated from a Ti:sapphire regenerative amplifier system (Micra-Legend Elite, Coherent Inc.), which is split into two beams; one is transformed into THz signal, passing <110> ZnTe crystal with a thickness of 1 mm and the other is maintained as a probe beam with a time delay by moving the delay stage. The former of THz signal is transmitted throughout the sample, and then detected by means of an electro-optic (EO) sampling method of 3 mm thick <110> ZnTe nonlinear crystal, which signal is collected with a lock-in amplifier (Stanford Research System, SR830). For OPTP measurement, the maximum point of the transmitted THz signal is verified and probe beam is positioned at this point by fixing the delay stage. The optical pump beam excites the samples with the time delay and transient change of the sample in the 0.2–2.6 THz frequency range was probed by THz probe pulse via EO sampling. The diameter of the pump beam is 3 mm, which is over two times larger than that of the THz probe beam. Thus, the time evolution of the pump-probe signal can be collected by scanning the time delay of the pump pulses with respect to the THz pulse. All OPTP experiments are carried out at room temperature in confined area by purging dry air.

2. Ultrafast carrier dynamics of CIGS solar cell

2.1. Na effect in CIGS solar cell

In CIGS solar cell, Na supply is known to be one of the methods for enhancing solar cell efficiency. Na atoms are typically supplied by utilizing SLG, which is a preferred substrate material for the industrial manufacturing of rigid CIGS-based modules. It is a generally accepted contention that Na atoms diffuse from the SLG into the CIGS layer through a Mo layer during fabrication of solar cell, beneficially affecting the conversion efficiency of the solar cell [20–24]. On the basis of Na effect, we assume that Na diffusion into the CIGS layer may alter the electronic structure and defect states. However, direct evidence of how Na influences the performance of solar cell has not yet been obtained experimentally. We consider the possibility that electronic structure of abundant defect states existed in the CIGS layer can be changed by Na content, which is a crucial issue in efforts to optimize solar cell design.

In this section, to investigate the formation of defect states in the CIGS layer depending on the Na content, the study of ultrafast carrier dynamics was conducted on the CIGS layers grown on two different substrates, borosilicate (BS) and SLG by measuring OPTP spectroscopy. Carrier dynamics related to defect states can be determined by the relaxation times of photoexcited carriers relative to the scattering rate or carrier-trapping at defect states, ranging from hundreds of *f*s to several *p*s. After p-n junction was formed by depositing a CdS layer as a buffer layer, carrier dynamics were also subsequently analyzed.

2.1.1. The fabrication of CIGS solar cell depending on Na content

CIGS layers of approximately 2.5 μm thick were deposited on Mo coated BS (Na_2O: 4 at.%) and SLG (Na_2O: 14 at.%), respectively. The Ga/III and Cu/III composition ratios of the CIGS layer were about 0.14 and 0.87 in both cases. As a buffer layer, an n-type CdS layer with a thickness of ~70 nm was grown on the CIGS via CBD method. Typical solar cells (ITO/i-ZnO/CdS/CIGS/Mo) were then fabricated on BS and SLG under identical conditions, and their efficiencies were determined to be 8.5 and 10.9%, respectively. The device performance on SLG was superior to that on BS by ~2.4%, which is ascribed to the diffusion of Na atoms from the SLG. To investigate how the substrates affected defect states, PL and OPTP measurements were conducted on CIGS and CdS/CIGS layers directly grown on BS and SLG without a Mo layer. For OPTP measurement, metal layer such as Mo should be removed because THz probe pulse can be easily absorbed by metal layer due to numerous free carriers.

SEM measurement was performed on each CdS/CIGS samples grown on BS and SLG as shown in **Figure 3a, b** and **c, d**, respectively. Approximately 2.5 μm thick CIGS absorber and 70 nm thick CdS buffer layer were similarly deposited on both substrates. We found out that grain size of CIGS grown on SLG is larger than that on BS, which is considered as diffused-Na from the SLG. To verify the existence of the Na content, depth profiles of the elemental constituents in the CdS/CIGS layer grown on BS and SLG were examined by using secondary ion mass spectroscopy (SIMS) as shown in **Figure 4**. A substantial Na content diffused up to the CdS layer in the SLG case, but not the BS. SIMS results clearly demonstrate that the SLG can effectively supply Na atoms into the CIGS and the CdS layer as compared to BS.

http://dx.doi.org/10.5772/66350

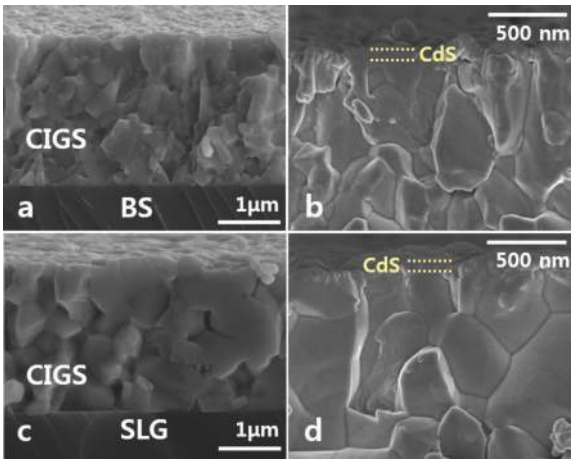

Figure 3. SEM images of CdS/CIGS film grown on BS (a, b) and SLG (c, d).

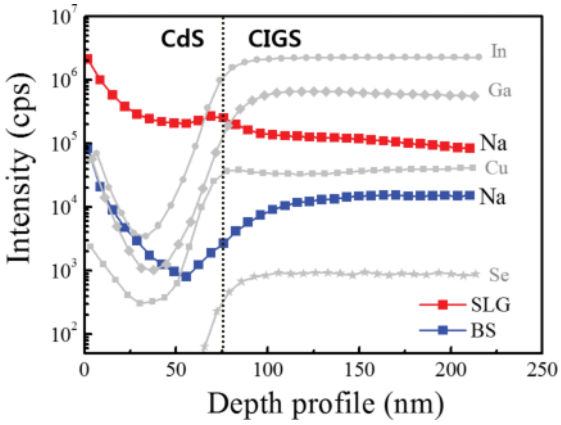

Figure 4. SIMS depth profiles of Na atoms in the CdS/CIGS layers grown on BS and SLG.

2.1.2. OPTP spectroscopy results

To measure the photoexcited carrier dynamics, the measurement of THz-TDs is essential. **Figure 5** shows the THz pulse spectra transmitted through the CIGS films grown on BS and SLG. After penetration of THz pulse through the samples, the intensity of THz pulse was drastically decreased as compared with the reference THz pulse (noted as "air").

Based on the results of THz-TDs spectrum, the measurement of OPTP spectroscopy was conducted on the CIGS and CdS/CIGS layer. In this experiment, pump beam of 400 nm is utilized

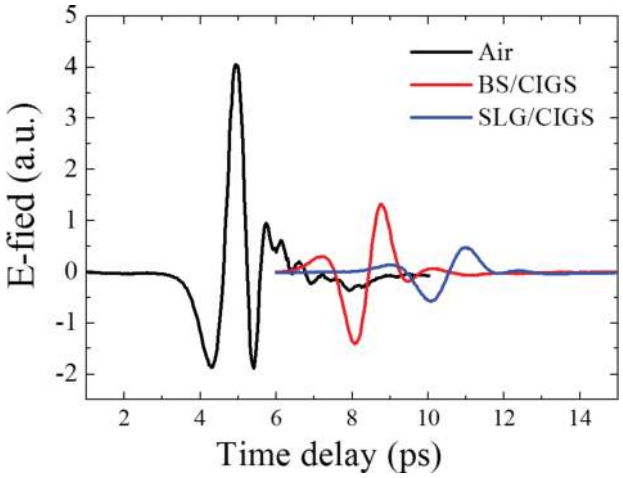

Figure 5. THz pulse spectra transmitted through the CIGS films grown on BS and SLG with a reference THz pulse measured by THz-TDs spectroscopy.

to excite photocarriers from the CdS buffer layer. When an intense *f*s laser pump pulse of 400 nm is injected, charge carriers excite, and the THz probe pulse is transmitted with pump-induced change; that is, the THz probe pulse transmitted through the samples reflects the absorption change induced by the *f*s laser pump pulse of 400 nm, which is expressed with, −ΔT/T. Thus, the near-edge −ΔT/T spectra intensity implies the photoexcited carrier density, and the decay curve corresponds to the carrier lifetime. The −ΔT/T signal is mainly attributed to the carrier relaxation of photoexcited electrons not holes since the effective mass of the electron is smaller than that of a hole in $CuInSe_2$ and $CuGaSe_2$ [9]. The typical −ΔT/T curve, at first, abruptly increases due to the absorption of photoexcited carriers by photon energy above the E_g, and then sequentially decays owing to the intraband relaxation (τ_1) and the recombination process/trapping at defect states (τ_2) [18, 25]. The photocarrier density is drastically decreased

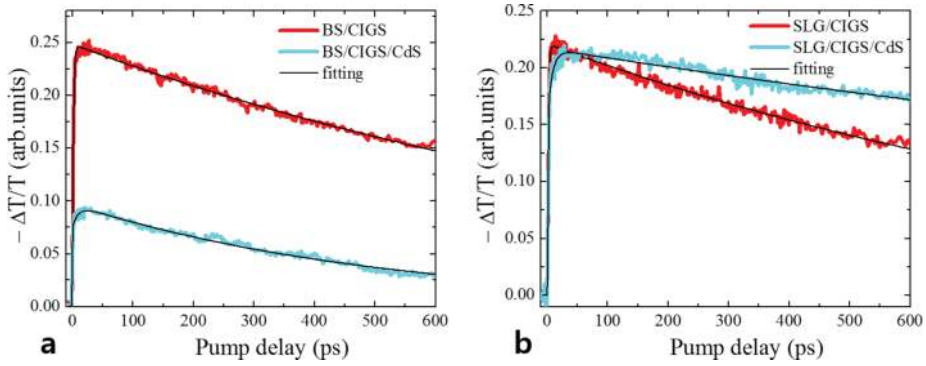

Figure 6. The measured and fitted −Δ*T*/*T* spectra of the CIGS and CdS/CIGS layers grown on BS (a) and SLG (b) produced by the photoinduced change in the THz probe pulse (a 400 nm pump beam was used).

http://dx.doi.org/10.5772/66350

	BS/CIGS	BS/CIGS/CdS	SLG/CIGS	SLG/CIGS/CdS
τ_1	1.7 ps	9.3 ps	1.3 ps	7.6 ps
τ_2	1150 ps	520 ps	1110 ps	2580 ps

Table 1. The carrier lifetimes obtained from the CdS/CIGS and CIGS layer are summarized as a function of substrate.

after the deposition of CdS layer in case of BS (**Figure 6a**) and is almost identical to both CIGS and CdS/CIGS layers in case of SLG (**Figure 6b**), which means that the characteristics of the CIGS layer is significantly changed in contact with the CdS layer. The time evolution of $-\Delta T/T$ can be well fitted with a biexponential function. The lifetimes of τ_1 and τ_2 obtained from the CIGS layer were approximately 1.7 and 1150 ps in BS, and 1.3 and 1110 ps in SLG; this means that a similar relaxation mechanism exists in the two CIGS layers. After deposition of the CdS layer, the lifetimes of τ_1 and τ_2 were noticeably changed, into 9.3 and 520 ps in BS, and 7.6 and 2580 ps in SLG. Interestingly, τ_2 dropped by half in BS, whereas it rose two-fold in SLG. These lifetimes are summarized in **Table 1**.

2.1.3. Ultrafast carrier dynamics at p-n junction of CdS/CIGS depending on Na content

To identify the defect states determining the lifetime of the relaxed carriers, PL measurement was performed with an excitation light of 400 nm, an identical value to the pump beam energy of OPTP measurement. PL peak assigned to the donor-acceptor pair (DAP) transition [26–29]. The DAP transition energy is measured of approximately 0.97 and 0.92 eV in CIGS on SLG and BS, respectively. Using the estimated E_g of 1.1 eV, the sum of each donor and acceptor ionization energy ($\Delta E_D + \Delta E_A$) becomes 130 meV in SLG and 180 meV in BS. According to several reports, the enthalpy of the formation energy of defects such as V_{Cu}, V_{Se}^+, and In_{Cu}^+ is very small and even negative [9, 30]. In the CIGS layer on SLG, the PL peak of 0.97 eV stems from the optical transition between the shallow acceptor level of 50 meV formed by V_{Cu} and the donor level of 80 meV created by Se vacancy (V_{Se}) [28]. In CIGS on BS, a new defect level emerges. It is plausible to assign this as an optical transition from antisite In_{Cu} as a donor level of descending order to V_{Cu} [28, 31].

Generally, photocarriers excited by high photon energy comply with Fermi-Dirac distributions through carrier-carrier scattering within a few hundred *f*s, and then lose their excess energy to the lattice, and relax to the bottom of the band by carrier-phonon scattering within several *p*s [18, 25]. In the both cases of CIGS on BS and SLG, τ_1 shows the similar trend regardless of substrate types because τ_1 is determined by the intraband relaxation time to reach the bottom of the conduction band; that is, it means that CIGS layers grown on BS and SLG are almost identical. Moreover, measured lifetimes of τ_1 in our system are similar to other results for CIGS thin film [32, 33]. On the other hand, τ_2 corresponds to an interband relaxation time either by the recombination of the electron-hole pair to restore initial states or by the electron trapping at defect states energetically located within the E_g. The both τ_2 obtained from the CIGS on BS and SLG also indicate similar values. Considering reported lifetimes, τ_2 is ascribed to the relaxation time from conduction band edge to the shallow acceptor energy level localized above the valence band edge within several nanoseconds [33]. After p-n junction is formed, τ_1 becomes longer within several picoseconds in both cases of CdS/CIGS on

BS and SLG. It is due to the CdS band structure with larger E_g of 2.4 eV, bringing about rise of the time for photocarriers to reach the conduction band edge. On the other hand, τ_2 exhibited the opposite trend after the deposition of the CdS layer on CIGS, which implies that different defect states are formed near the p-n junction as a function of substrate type. In BS, τ_2 is about 520 ps, whereas in SLG, it is approximately 2580 ps; that is, in the case of BS, a deeper defect level to trap photocarriers could be formed at the p-n junction, shortening τ_2 value. Considering PL results, the formation of deeper defect states into the E_g is plausible in CIGS on BS because decreased PL intensity in BS is caused by electron trapping at defect states instead of the radiative recombination. We suggest that the Na atoms affect the quality of p-n junctions and defect states located in E_g. According to calculation results, ionized intrinsic In_{Cu}^{2+} can transform into lattice-relaxed, deep defect level "*DX* states" formed as a Frenkel-pair consisting of an In interstitial and a Cu vacancy; that is, $In_{Cu}^{2+} + 2e \rightarrow In_{DX}^{0} = (In_i^{+} - V_{Cu}^{-})$ [34]. Since large quantities of isolated In_{Cu} and isolated V_{Cu} are formed very close to a 1:2 ratio during CIGS growth, most In_{Cu} eventually exists as a neutral defect ($In_{Cu} - 2V_{Cu}$), whereas the amount of uncompensated isolated In_{Cu} becomes a donor [35, 36]. The above intrinsic defect complexes can create the defect-localized states in the E_g, namely "*DX* states," in the case of $Cu(In_{1-x}Ga_x)Se_2$ with an $E_g \leq 1.2$ eV and $x < 0.3$ [34]. This has a harmful influence on PV device performance by trapping photocarriers produced by photoexcitation under illumination. These "*DX* states" even cause Fermi level pinning and trapping of photocarriers near the p-n junction, resulting in a decrease of τ_2 in BS. In the case of SLG, the increase of τ_2 is thought to result because the added Na automatically diffuses into the CIGS and CdS layer from the SLG, as demonstrated in SIMS results. The incorporation of less than 1% Na is considered enough to significantly change their electronic properties. Na is known to reduce the defect density inCIGS film by passivation of the Se vacancy or annihilation of the compensating antisite donor defect In_{Cu} by Na [20]. We suggest a possible scenario for the cause of the longer lifetime, τ_2 in SLG: (i) Na eliminates In_{Cu} by substituting for In on Cu sites; that is, forming Na_{Cu} and (ii) Na easily forms Na_{In} antisites defects, resulting in an increase in acceptor density. Thus, there is no "*DX* state" in SLG, which is due to the deficient In_{Cu} being replaced by Na_{Cu} which prevents the creation of defect complexes ($In_{Cu} - 2V_{Cu}$), near the p-n junction. In other words, the introduction of Na into the CIGS and CdS layers plays an important role in the PV device; this is because of the removal of "*DX* states" and an increase in acceptors, thereby promoting τ_2 in SLG. The relaxation mechanism of photocarriers at the p-n junction of CdS/CIGS depending on the two substrates of BS and SLG is displayed in a simplified band structure in **Figure 7**. This result clearly indicates that Na atoms exert a positive effect at the p-n junction of PV devices by producing increased photocarrier lifetimes in the case of SLG.

2.2. Variation of buffer layer in CIGS solar cell

Typical CIGS-based solar cells have a buffer layer between the CIGS absorber layer and the transparent ZnO front electrode, which plays an important role in improving the cell performance. Among various buffer materials, Zn-based materials have been frequently studied because of their beneficial properties, for example, good transparency with large direct E_g, less toxicity, and cost effectiveness [37–40]. ZnS film can be grown by various deposition methods such as evaporation, atomic layer deposition, sputtering, and metal organic chemical vapor

http://dx.doi.org/10.5772/66350

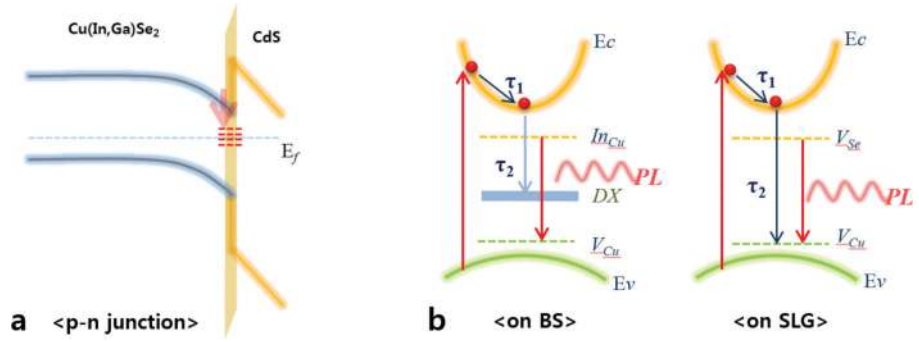

Figure 7. (a) A schematic defect level diagram at the p-n junction of CdS/CIGS. (b) Illustration of the carrier relaxation mechanism of CIGS thin films after deposition of CdS layer depending on substrate type of BS and SLG.

deposition. The efficiency of the CIGS solar cell with a Zn-based buffer layer is comparable to a conventional CIGS solar cell with a CdS buffer layer [41]. Ultimately, the efficiency of solar cells with a Zn-based buffer layer depends on the properties of the p-n junction, which is mainly determined by the buffer layer deposition process.

In this section, we fabricated a CIGS solar cell with Zn-based buffer layers grown by three deposition methods, cracker-Zn(O,S), CBD-Zn(O,S), and sputter-Zn(O,S), based on optimized conditions previously determined by our group [42–45]. To extract the correlation between cell efficiency and the interfacial characteristics between the CIGS and buffer layer, OPTP spectroscopy was utilized to investigate the CIGS, and the CIGS with the buffer layer, with respect to carrier trapping times at defect states.

2.2.1. The fabrication of a CIGS solar cell with a Zn-based buffer layer

A CIGS layer of approximately 2.2 μm thick was deposited on a Mo coated SLG. The Ga/III and Cu/III composition ratios of the CIGS layer were measured to be about 0.3 and 0.96, respectively, by X-ray fluorescence. We prepared two vacuum-based buffer layers of cracker-Zn(O,S) and sputter-Zn(O,S) with thicknesses of ~8 and 70 nm, respectively. We also arranged one chemical-based buffer layer of CBD-Zn(O,S) with a thickness of 30 nm. Since the buffer layers were deposited utilizing the optimized conditions from our group, their thicknesses were different.

Typical solar cells were fabricated with the various buffer layers, and the other deposition conditions were identical. The performance of the solar cell showed that the results depend on the buffer types. The best cell efficiency of approximately 13% was obtained for the CIGS solar cell with CBD-Zn(O,S).

Details of the cell structures and their cell performance are provided in **Figure 8**. For the OPTP measurement, CIGS without a Mo layer and a Zn-based buffer layer was directly deposited on SLG, and the injected and transmitted optical and THz pulses are simply illustrated in **Figure 9**.

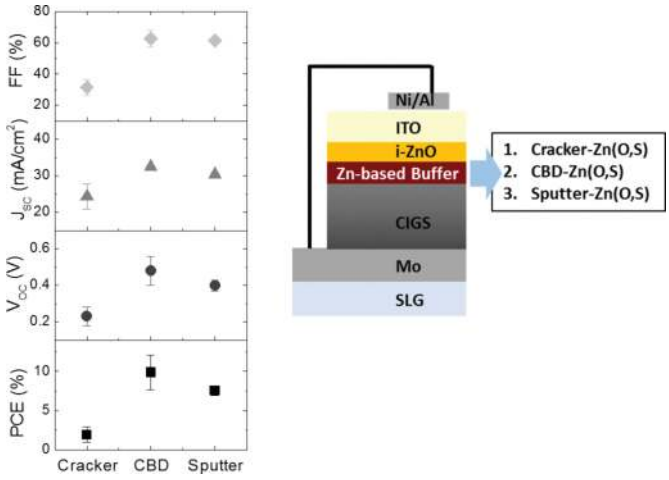

Figure 8. The performance of the CIGS solar cell as a function of the method of deposition of the Zn-based buffer layer (left), and an illustration of the completed CIGS solar cell structure (right).

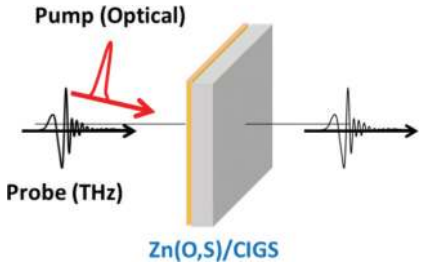

Figure 9. Simplified schematic diagram of the OPTP spectroscopy measurement.

2.2.2. OPTP spectroscopy results

For OPTP measurement, THz-TDs were conducted on the samples by comparing the THz pulse before and after transmission through the sample. **Figure 10a** shows the THz pulse spectra transmitted through the SLG, which is drastically reduced in comparison with the reference THz pulse through "air". After penetration of the THz pulse through the sample of CIGS and the Zn(O,S) buffer layers deposited on the CIGS, the intensity of the THz pulses were found to be similar to each other, as indicated in **Figure 10b**. This means that no photo-carriers were excited by the THz pulse.

Based on the results of the THz-TDs spectra, OPTP spectroscopy measurements were carried out on the CIGS and Zn(O,S)/CIGS layers. In those experiments, two pump beams of 400 and 800 nm were used to investigate optically photoexcited carrier dynamics along the depth distribution.

http://dx.doi.org/10.5772/66350

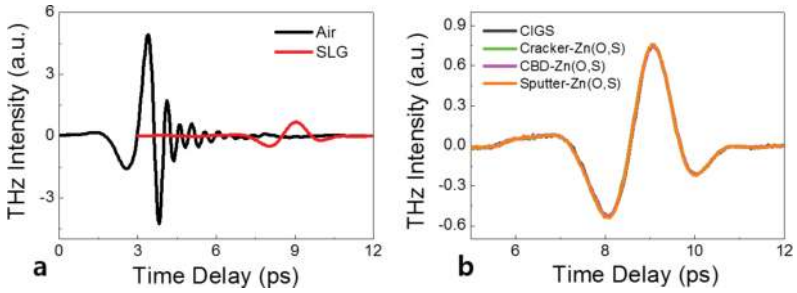

Figure 10. THz pulse spectra transmitted through the SLG and air (as a reference) (a), and CIGS and Zn(O,S) buffer layers/CIGS grown on SLG (b) measured by THz-TDs.

Figure 11a and **b** show the $-\Delta T/T$ spectra and normalized ΔT spectra of the CIGS film as a function of pump beam energy. The spectra intensity at the near-edge implies the photoexcited carrier density, and the decay curve corresponds to the carrier lifetime. In the CIGS film, the photoexcited carrier density and carrier lifetime were drastically increased by the pump beam of 800 nm, as compared with the 400 nm beam, which means that the density of defect states in the CIGS is differentiated along the depth direction.

Considering the penetration depth of the pump beam into the CIGS film, a wavelength of 400 nm should penetrate the surface of the CIGS less than 50 nm, and the 800 nm beam should reach the near-surface of the CIGS at about 150 nm. Thus, we assume that the charge carrier density acting as long-lived photocarriers is higher at the near-surface than the surface of the CIGS.

To extract carrier lifetimes relative to defect states, we fitted the normalized ΔT spectra of the CIGS using the equation (1) that follows:

$$y(t) = [A_e \cdot (\mathrm{erf}\left(\frac{t-t_e}{-\tau_e}\right) + y_e)] \times [A_0 \cdot \exp\left(\frac{t-t_0}{-\tau_0}\right) + A_1 \cdot \exp\left(\frac{t-t_0}{-\tau_1}\right) + A_2 \cdot \exp\left(\frac{t-t_0}{-\tau_2}\right)] \quad (1)$$

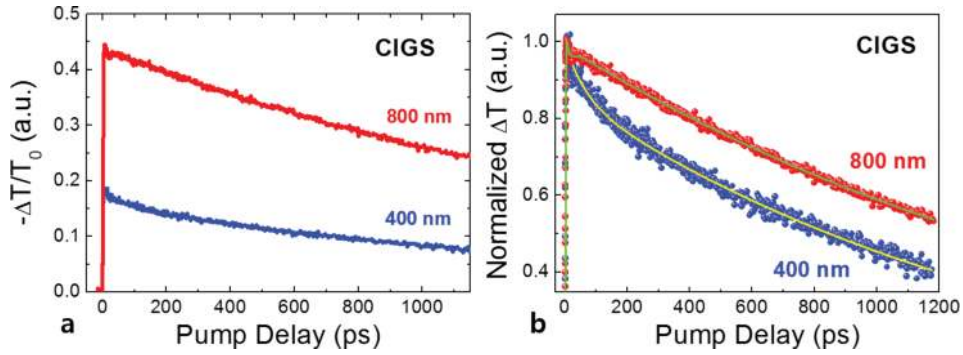

Figure 11. The measured $-\Delta T/T$ spectra of the CIGS (a) and normalized ΔT spectra of the CIGS (b) as a function of pump beam energies of 400 and 800 nm.

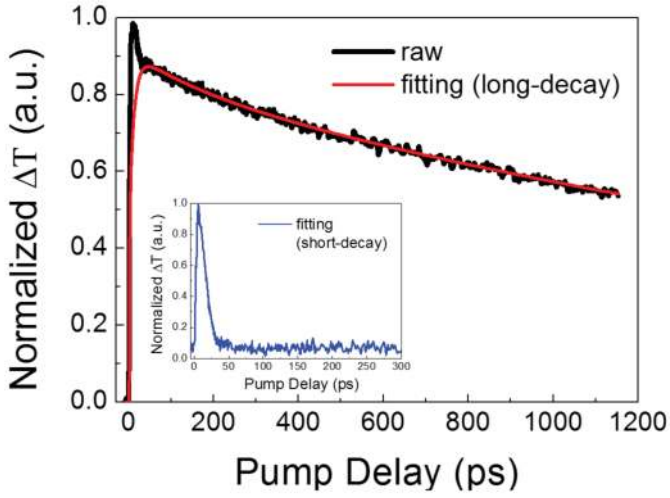

Figure 12. The normalized and fitted ΔT spectra of the CIGS measured at a pump beam energy of 800 nm. This indicates the fitting method, after subtracting the short decay curves caused by the sharp peak.

In this study, a sharp peak appeared at the near-edge of the normalized ΔT spectra with the 800 nm pump beam (**Figure 11b**), which was separately fitted, as indicated in **Figure 12**. To consider only the long decay curve while excluding the very sharp peak, we subtracted the very short decay curves of less than 1 *p*s by fitting, as indicated in the inset of **Figure 12**. From the fitting results, the notable thing to be observed is that the fast carrier lifetime (τ_1) of 61.8 *p*s and the long carrier lifetime (τ_2) of 1552 *p*s existed for the 400 nm pump beam, while τ_1 disappeared and τ_2 became longer, reaching 1930 *p*s for the 800 nm pump beam.

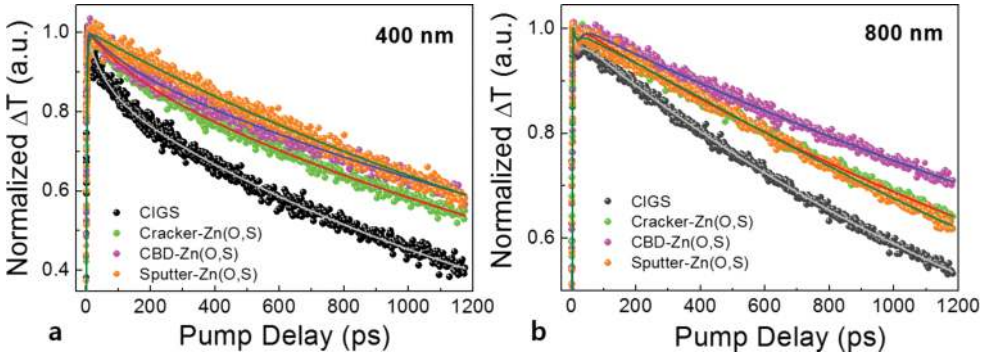

Figure 13. The normalized and fitted ΔT spectra of the pure CIGS film and various Zn(O,S) buffer layers deposited on CIGS film, as a function of pump beam energies of 400 nm (a) and 800 nm (b).

http://dx.doi.org/10.5772/66350

After deposition of the Zn(O,S) buffer layers on the CIGS film, OPTP spectroscopy was also conducted. The photoexcited carrier density and carrier lifetimes at 800 nm were much higher than that at 400 nm, which is a similar tendency to the measured spectra from the CIGS films as shown in **Figure 11a**. After depositing the buffer layer on the CIGS, the decay curves were extended regardless of the deposition method of buffer layer for both the 400 and 800 nm pump beams.

To clearly express the distinctive features of the carrier lifetimes according to buffer types, we fitted the normalized ΔT spectra as presented in **Figure 13a** and **b**. The detailed carrier lifetimes obtained from the fitting results are summarized in **Table 2**. After deposition of the Zn(O,S) buffer layers, two carrier lifetimes of τ_1 and τ_2 existed for the 400 nm pump beam, whereas only the τ_2 value was detected and prolonged for the 800 nm pump beam, as was the case with CIGS. In the case of the sputter-Zn(O,S)/CIGS, only the τ_2 value was found, without τ_1, irrespective of pump beam energy.

Pump beam energy	Lifetimes	CIGS	Cracker	CBD	Sputter
400 nm	τ_1 (ps)	61.8	141	119	-
	τ_2 (ps)	1552	2171	2529	2212
800 nm	τ_1 (ps)	-	-	-	-
	τ_2 (ps)	1930	2611	3325	2500

Table 2. The carrier lifetimes obtained from the pure CIGS film and various Zn(O,S) buffer layers grown on CIGS film are summarized as a function of pump beam energy.

2.2.3. Ultrafast carrier dynamics of the CIGS/Zn-based buffer layer

To investigate the carrier dynamics related to the defect states along the depth direction in the CIGS and Zn(O,S)/CIGS, 400 and 800 nm pump beam energies were applied. The 400 nm pump beam is sensitive to the surface of the film, and the 800 nm pump beam reflects from the near-surface of the film. The photocarriers in the CIGS film can be excited by both pump beams, whereas those of the Zn(O,S) film cannot be excited by the 800 nm pump beam due to its low energy of 1.55 eV.

To verify the light absorption of the Zn(O,S) buffer layer at the 800 nm wavelength depending on the deposition method, transmittance spectra were measured for various Zn(O,S) films directly grown on SLG, as indicated in **Figure 14**. After deposition of the Zn(O,S) film, the wavelength of 800 nm mostly penetrated toward the CIGS film.

In the pure CIGS film, two carrier lifetimes (fast: τ_1 of 61.8 *p*s and long: τ_2 of 1552 *p*s) were detected for the 400 nm pump beam, while the fast carrier lifetime τ_1 was dissipated and long carrier lifetime τ_2 was prolonged to 1930 *p*s for the 800 nm pump beam. From these results, we inferred that there were different defect states available to trap photoexcited carriers at the surface and the near-surface, respectively.

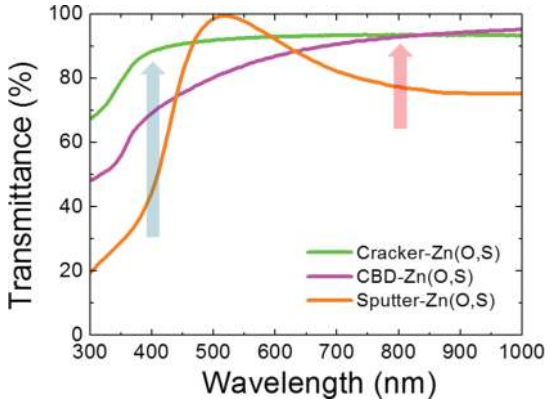

Figure 14. Transmittance spectra of various Zn(O,S) films grown on SLG.

Even though there are several defect levels in the E_g of CIGS, the carrier lifetimes average out to one decay time. Thus, τ_1 and τ_2 should be explained with different photocarrier trapping times, not defect energy levels. A typical CIGS film consists of numerous defect states, caused by several point defects, grain boundaries, and rough surface [7, 9, 34]. With the injection of the 400 nm pump beam into the CIGS film, the rough surface is an important factor, because in a semiconductor, photocarriers can be captured at surface defect states.

Among the several point defects that exist in the CIGS film, Cu vacancies (V_{Cu}) can be easily formed due to their low formation energy, creating a shallow acceptor level [9]. Thus, the V_{Cu} defect level can have a dominant role in the trapping of photoexcited electrons. (In the OPTP experiments, we only considered photoexcited electrons, not holes, due to the higher mobility of photoexcited electrons as compared to photoexcited holes.) Considering that photocarriers are primarily excited in the surface region for the 400 nm, the trapping time of the surface defect states is relatively faster than the bulk defects of V_{Cu}. Based on surface defects and V_{Cu}, we assumed that τ_1 and τ_2 correspond to the trapping times of photoexcited electrons in the surface defect states, and the V_{Cu} defects entirely distributed from surface to bulk, respectively.

With the injection of the 800 nm pump beam into the CIGS film, photoexcited electrons occur at the near-surface, and not the surface. Thus, τ_1 reflecting the CIGS surface is not detected, because the photoexcited electrons are dominantly captured at bulk defect states before being trapped at the surface defect states. The lower the defect density, the more that carrier lifetime is increased. Here, τ_2 is increased as compared to that for the 400 nm pump beam, which means that the bulk defect density, V_{Cu}, decreases along the depth direction, resulting in a rise in τ_2. The carrier dynamics model in the pure CIGS film is illustrated in **Figure 15a**.

After deposition of the Zn(O,S) buffer layers on the CIGS film, both τ_1 and τ_2 were increased for the 400 nm pump beam, excluding the sputter-Zn(O,S) buffer layer. The increase in τ_1 is attributed to the surface curing effect, which reduces surface defect states after the deposition of the buffer layer. Since a thin-buffer layer does not entirely cover the rough surface of

http://dx.doi.org/10.5772/66350

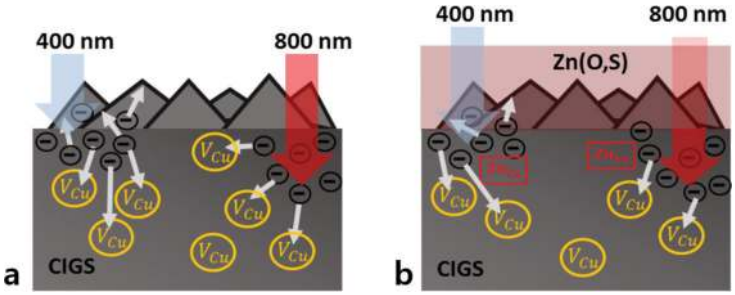

Figure 15. Schematic diagram of photoexcited carrier dynamics in the pure CIGS film (a) and after deposition of Zn(O,S) buffer layers on the CIGS film (b) as a function of pump beam energy.

the CIGS film, τ_1 is slightly increased up to ~140 *p*s and 120 *p*s in cracker-Zn(O,S) and CBD-Zn(O,S) which are about 8 and 30 nm thick, respectively.

In the sputter-Zn(O,S) buffer layer, τ_1 is dissipated because of its thick-film thickness of 70 nm, which relieves the surface scattering effect, as compared with the other buffer layers. In general, Zn atoms of the buffer layer have been known to diffuse toward the CIGS film. The diffused Zn atoms can occupy the V_{Cu} sites, forming a Zn^+ charge state as a donor [46, 47]. Thus, Zn substitution to V_{Cu}, Zn_{Cu}, causes a reduction in the bulk defect states available to trap photoexcited electrons, resulting in a rise of τ_2.

With the 800 nm pump beam, τ_1 also disappeared, like the CIGS film, implying surface defect states were not detected. The τ_2 values also increased, which is ascribed to the combination of increased Zn_{Cu} in the surface region of the CIGS, and decreased bulk defect density, V_{Cu}.

The carrier dynamics model in the Zn(O,S)/CIGS film is illustrated in **Figure 15b**. τ_2 showed the highest values for both pump beams of 400 and 800 nm in the CBD-Zn(O,S) buffer layer grown on CIGS, as compared with the others. From these results, we carefully suggest that solar cell efficiency can be enhanced when carrier lifetime reflecting bulk defect density is prolonged.

3. Conclusion

In summary, we have demonstrated the effectiveness of OPTP measurement for determining the ultrafast carrier dynamics of photocarriers excited from CIGS and buffer layers, depending on substrate type (BS and SLG) and several Zn(O,S) buffer layers (cracker-, CBD-, sputter-Zn(O,S)). By fitting the normalized ΔT spectra, carrier lifetimes were extracted and then carrier behavior was analyzed, related with defect states.

Considering the enthalpy of formation energy, V_{Cu} can be easily formed in CIGS, which has an important influence on carrier lifetimes. In the first study, we found that a deep complex defect level of ($In_{Cu} - 2\,V_{Cu}$), designated "*DX* states," could be natively formed in the E_g near the p-n junction in the case of BS, resulting in a decrease of τ_2 due to trapping photocarriers.

In contrast, τ_2 was increased in SLG with the addition of a Na supply, which is considered to relieve the defect level located in the E_g, forming the Na_{Cu}, antisite.

In the second study, the behavior of V_{Cu} defect states was determined to play a dominant role. Based on the geometric characteristics of the CIGS layer, we defined the two types of defect states, τ_1 and τ_2, which correspond to the trapping times of photoexcited electrons in the surface defect states at the CIGS surface, and the V_{Cu} defects, which are entirely distributed in the CIGS bulk, respectively. From the fitted τ_1 and τ_2 values, we discovered that the V_{Cu} defect states decrease in the depth direction of the CIGS, and Zn substitution to V_{Cu}, Zn_{Cu}, causes a decrease in bulk defect states available to trap photoexcited electrons, resulting in a rise of τ_2.

Acknowledgements

This work was supported by the "New & Renewable Energy" project of the Korea Institute of Energy Technology Evaluation and Planning (KETEP) grant funded by the Korean government Ministry Of Trade, Industry, & Energy (20153010011990, 20153000000030). The authors also would like to acknowledge the financial support from the R&D Convergence Program of MSIP (Ministry of Science, ICT and Future Planning) and ISTK (Korea Research Council for Industrial Science and Technology) of the Republic of Korea (Grant B551179-12-01-00).

Author details

Woo-Jung Lee and Yong-Duck Chung*

*Address all correspondence to: ydchung@etri.re.kr

Electronics and Telecommunications Research Institute, Daejeon, Korea

References

[1] Andrew M. Gabor, John R. Tuttle, David S. Albin, Miguel A. Contreras, Rommel Noufi, and Allen M. Hermann: High-efficiency $CuIn_xGa_{1-x}Se_2$ solar cells made from $(In_xGa_{1-x})_2Se_3$ precursor films. Applied Physics Letters. 1994; **65**: 198–200. DOI: 10.1063/1.112670

[2] Clas Persson, Yu-Jun Zhao, Stephan Lany, and Alex Zunger: n-type doping of $CuInSe_2$ and $CuGaSe_2$. Physical Review B. 2005; **72**: 035211. DOI: 10.1103/PhysRevB.72.035211

[3] Ingrid Repins, Miguel A. Contreras, Brian Egaas, Clay DeHart, John Scharf, Craig L. Perkins, Bobby To, and Rommel Noufi: 19.9%-efficient ZnO/CdS/$CuInGaSe_2$ solar cell with 81.2% fill factor. Progress in Photovoltaics: Research and applications. 2008; **16**: 235–239. DOI: 10.1002/pip.822

[4] Philip Jackson, Dimitrios Hariskos, Erwin Lotter, Stefan Paetel, Roland Wuerz, Richard Menner, Wiltraud Wischmann, and Michael Powalla: New world record efficiency for Cu(In,Ga)Se_2 thin-film solar cells beyond 20%. Progress in Photovoltaics: Research and Applications. 2011; **19**: 894–897. DOI: 10.1002/pip.1078

[5] Philip Jackson, Roland Wuerz, Dimitrios Hariskos, Erwin Lotter, Wolfram Witte, and Michael Powalla: Effects of heavy alkali elements in Cu(In,Ga)Se_2 solar cells with efficiencies up to 22.6%. Physica Status Solidi (RRL)-Rapid Research Letters. 2016; 10: 583–586 DOI: 10.1002/pssr.201600199

[6] B Ohnesorge, R Weigand, G Bacher, A Forchel, W Riedl, and FH Karg: Minority-carrier lifetime and efficiency of Cu(In,Ga)Se_2 solar cells. Applied Physics Letters. 1998; **73**: 1224–1226. DOI: 10.1063/1.122134

[7] Michael Hafemeister, Susanne Siebentritt, Jürgen Albert, Martha Ch Lux-Steiner, and Sascha Sadewasser: Large neutral barrier at grain boundaries in chalcopyrite thin films. Physical Review Letters. 2010; **104**: 196602. DOI: 10.1103/PhysRevLett.104.196602

[8] Harry Mönig, Y Smith, Raquel Caballero, Christian Kaufmann, Iver Lauermann, Martha ch. Lux-Steiner, and Sascha Sadewasser: Direct evidence for a reduced density of deep level defects at grain boundaries of Cu(In,Ga)Se_2 thin films. Physical review letters. 2010; **105**: 116802. DOI: 10.1103/PhysRevLett.105.116802

[9] Shengbai Zhang, Su-Huai Wei, Alex Zunger, and H Katayama-Yoshida: Defect physics of the $CuInSe_2$ chalcopyrite semiconductor. Physical Review B. 1998; **57**: 9642. DOI: 10.1103/PhysRevB.57.9642

[10] Yong-Duck Chung, Dae-Hyung Cho, Won-Seok Han, Nae-Man Park, Kyu-Seok Lee, and Jeha Kim: Incorporation of Cu in Cu(In,Ga)Se_2-based thin-film solar cells. Journal of the Korean Physical Society. 2010; **57**: 1826–1830. DOI: 10.3938/jkps.57.1826

[11] Dae-Hyung Cho, Yong-Duck Chung, Kyu-Seok Lee, Nae-Man Park, Kyung-Hyun Kim, Hae-Won Choi, and Jeha Kim: Influence of growth temperature of transparent conducting oxide layer on Cu(In,Ga)Se_2 thin-film solar cells. Thin Solid Films. 2012; **520**: 2115–2118. DOI: 10.1016/j.tsf.2011.08.083

[12] Jae-Hyung Wi, Woo-Jung Lee, Dae-Hyung Cho, Won Seok Han, Jae Ho Yun, and Yong-Duck Chung: Characteristics of temperature and wavelength dependence of $CuInSe_2$ thin-film solar cell with sputtered Zn(O,S) and CdS buffer layers. physica status solidi (a). 2014; **211**: 2172–2176. DOI: 10.1002/pssa.201431232

[13] Katsumi Kushiya and Osamu Yamase: Stabilization of PN heterojunction between Cu(InGa)Se_2 thin-film absorber and ZnO window with Zn(O,S,OH)x buffer. Japanese Journal of Applied Physics. 2000; **39**: 2577. DOI: 10.1143/JJAP.39.2577

[14] Taizo Kobayashi, Hiroshi Yamaguchi, and Tokio Nakada: Effects of combined heat and light soaking on device performance of Cu(In,Ga)Se_2 solar cells with ZnS(O,OH) buf-

fer layer. Progress in Photovoltaics: Research and Applications. 2014; **22**: 115–121. DOI: 10.1002/pip.2339

[15] Negar Naghavi, Solange Temgoua, Thibaud Hildebrandt, Jean François Guillemoles, and Daniel Lincot: Impact of oxygen concentration during the deposition of window layers on lowering the metastability effects in Cu(In,Ga)Se_2/CBD Zn(S,O) based solar cell. Progress in Photovoltaics: Research and Applications. 2015; **23**: 1820–1827. DOI: 10.1002/pip.2626

[16] Rohit P. Prasankumar, Prashanth C. Upadhya, and Antoinette J. Taylor: Ultrafast carrier dynamics in semiconductor nanowires. Physica Status Solidi (b). 2009; **246**: 1973–1995. DOI: 10.1002/pssb.200945128

[17] Priti Tiwana, Patrick Parkinson, Michael B. Johnston, Henry J. Snaith, and Laura M. Herz: Ultrafast terahertz conductivity dynamics in mesoporous TiO_2: influence of dye sensitization and surface treatment in solid-state dye-sensitized solar cells. The Journal of Physical Chemistry C. 2009; **114**: 1365–1371. DOI: 10.1021/jp908760r

[18] Ronald Ulbricht, Euan Hendry, Jie Shan, Tony F. Heinz, and Mischa Bonn: Carrier dynamics in semiconductors studied with time-resolved terahertz spectroscopy. Reviews of Modern Physics. 2011; **83**: 543. DOI: 10.1103/RevModPhys.83.543

[19] Woo-Jung Lee, Dae-Hyung Cho, Jae-Hyung Wi, Won Seok Han, Yong-Duck Chung, Jaehun Park, Jung Min Bae, and Mann-Ho Cho: Na-dependent ultrafast carrier dynamics of CdS/Cu(In,Ga)Se_2 measured by optical pump-terahertz probe spectroscopy. The Journal of Physical Chemistry C. 2015; **119**: 20231–20236. DOI: 10.1021/acs.jpcc.5b02282

[20] Leeor Kronik, David Cahen, and Hans Werner Schock: Effects of sodium on polycrystalline Cu(In,Ga)Se_2 and its solar cell performance. Advanced Materials. 1998; **10**: 31–36. DOI: 10.1002/(SICI)1521-4095(199801)10:1<31::AID-ADMA31>3.0.CO;2-3

[21] Dominik Rudmann, Antonio F. da Cunha, Marc Kaelin, Fe Kurdesau, Hans Zogg, Ayodhya N. Tiwari, and Gerhard Bilger: Efficiency enhancement of Cu(In,Ga)Se_2 solar cells due to post-deposition Na incorporation. Applied Physics Letters. 2004; **84**: 1129–1131. DOI: 10.1063/1.1646758

[22] Shogo Ishizuka, Akimasa Yamada, Muhammad Monirul Islam, Hajime Shibata, Paul Fons, Takeaki Sakurai, Katsuhiro Akimoto, and Shigeru Niki: Na-induced variations in the structural, optical, and electrical properties of Cu(In,Ga)Se_2 thin films. Journal of Applied Physics. 2009; **106**: 034908. DOI: 10.1063/1.3190528

[23] Dae-Hyung Cho, Kyu-Seok Lee, Yong-Duck Chung, Ju-Hee Kim, Soo-Jeong Park, and Jeha Kim: Electronic effect of Na on Cu(In,Ga)Se_2 solar cells. Applied Physics Letters. 2012; **101**: 023901. DOI: 10.1063/1.4733679

[24] Woo-Jung Lee, Dae-Hyung Cho, Jae-Hyung Wi, Won Seok Han, Jeha Kim, and Yong-Duck Chung: Na effect on flexible Cu(In,Ga)Se_2 photovoltaic cell depending on diffusion

barriers (SiOx, i-ZnO) on stainless steel. Materials Chemistry and Physics. 2014; **147**: 783–787. DOI: 10.1016/j.matchemphys.2014.06.021

[25] Andreas Othonos: Probing ultrafast carrier and phonon dynamics in semiconductors. Journal of Applied Physics. 1998; **83**: 1789–1830. DOI: 10.1063/1.367411

[26] Ingo Dirnstorfer, Mt. Wagner, Detlev M. Hofmann, MD Lampert, Franz Karg, and Bruno K. Meyer: Characterization of CuIn(Ga)Se_2 thin films. Physica Status Solidi (a). 1998; **168**: 163–175. DOI: 10.1002/(SICI)1521-396X(199807)168:1<163::AID-PSSA163>3.0.CO;2-T

[27] Rajmund Bacewicz, P. Zuk, and R. Trykozko: Photoluminescence study of ZnO/CdS/Cu(In,Ga)Se_2 solar cells. Optoelectronics Review. 2003; **11**: 277–280.

[28] Sho Shirakata, Katsuhiko Ohkubo, Yasuyuki Ishii, and Tokio Nakada: Effects of CdS buffer layers on photoluminescence properties of Cu(In,Ga)Se_2 solar cells. Solar Energy Materials and Solar Cells. 2009; **93**: 988–992. DOI: 10.1016/j.solmat.2008.11.043

[29] Young Min Shin, Chang Soo Lee, Dong Hyeop Shin, Young Min Ko, Essam A Al-Ammar, Hyuck Sang Kwon, and Byung Tae Ahn: Characterization of Cu(In,Ga)Se_2 solar cells grown on Na-free glass with an NaF layer on a Mo film. ECS Journal of Solid State Science and Technology. 2013; **2**: P248–P252. DOI: 10.1149/2.002306jss

[30] Su-Huai Wei, Shengbai Zhang, and Alex Zunger: Effects of Ga addition to $CuInSe_2$ on its electronic, structural, and defect properties. Applied Physics Letters. 1998; **72**: 3199–3201. DOI: 10.1063/1.121548

[31] S Zotta, Karl Leo, Martin Ruckh, and Hans Warner Schock: Photoluminescence of polycrystalline $CuInSe_2$ thin films. Applied Physics Letters. 1996; **68**: 1144–1146. DOI: 10.1063/1.115704

[32] Shih-Chen Chen, Yu-Kuang Liao, Hsueh-Ju Chen, Chia-Hsiang Chen, Chih-Huang Lai, Yu-Lun Chueh, Hao-Chung Kuo, Kaung-Hsiung Wu, Jenh-Yih Juang, and Shun-Jen Cheng: Ultrafast carrier dynamics in Cu(In,Ga)Se_2 thin films probed by femtosecond pump-probe spectroscopy. Optics Express. 2012; **20**: 12675–12681. DOI: 10.1364/OE.20.012675

[33] Makoto Okano, Yutaro Takabayashi, Takeaki Sakurai, Katsuhiro Akimoto, Hajime Shibata, Shigeru Niki, and Yoshihiko Kanemitsu: Slow intraband relaxation and localization of photogenerated carriers in $CuIn_{1-x}Ga_xSe_2$ thin films: Evidence for the existence of long-lived high-energy carriers. Physical Review B. 2014; **89**: 195203. DOI: 10.1103/PhysRevB.89.195203

[34] Stephan Lany and Alex Zunger: Intrinsic DX Centers in Ternary Chalcopyrite Semiconductors. Physical review letters. 2008; **100**: 016401. DOI: 10.1103/PhysRevLett.100.016401

[35] Yu-Jun Zhao, Clas Persson, Stephan Lany, and Alex Zunger: Why can $CuInSe_2$ be readily equilibrium-doped n-type but the wider-gap $CuGaSe_2$ cannot? Applied Physics Letters. 2004; **85**: 5860–5862. DOI: 10.1063/1.1830074

[36] Stephan Lany, Yu-Jun Zhao, Clas Persson, and Alex Zunger: Halogen n-type doping of chalcopyrite semiconductors. Applied Physics Letters. 2005; **86**: 42109–42109. DOI: 10.1063/1.1854218

[37] Tokio Nakada, Masayuki Mizutani, Y Hagiwara, and Akio Kunioka: High-efficiency Cu(In,Ga)Se_2 thin-film solar cells with a CBD-ZnS buffer layer. Solar Energy Materials and Solar Cells. 2001; **67**: 255–260. DOI: 10.1016/S0927-0248(00)00289-0

[38] Tokio Nakada and Masayuki Mizutani: 18% efficiency Cd-free Cu(In,Ga)Se_2 thin-film solar cells fabricated using chemical bath deposition (CBD)-ZnS buffer layers. Japanese Journal of Applied Physics. 2002; **41**: L165.

[39] Negar Naghavi, Stefani Spiering, Michael Powalla, Bruno Cavana, and Daniel Lincot: High-efficiency copper indium gallium diselenide (CIGS) solar cells with indium sulfide buffer layers deposited by atomic layer chemical vapor deposition (ALCVD). Progress in Photovoltaics: Research and Applications. 2003; **11**: 437–443. DOI: 10.1002/pip.50

[40] Muhammad Monirul Islam, Shogo Ishizuka, Akimasa Yamada, Keiichiro Sakurai, Shigeru Niki, Takeaki Sakurai, and Katsuhiro Akimoto: CIGS solar cell with MBE-grown ZnS buffer layer. Solar Energy Materials and Solar Cells. 2009; **93**: 970–972. DOI: 10.1016/j.solmat.2008.11.047

[41] Theresa Magorian Friedlmeier, Philip Jackson, Andreas Bauer, Dimitrios Hariskos, Oliver Kiowski, Roland Wuerz, and Michael Powalla: Improved photocurrent in Cu (In,Ga)Se_2 solar cells: from 20.8% to 21.7% efficiency with CdS buffer and 21.0% Cd-free. IEEE Journal of Photovoltaics. 2015; **5**: 1487–1491. DOI: 10.1109/JPHOTOV.2015.2458039

[42] Dae-Hyung Cho, Woo-Jung Lee, Sang-Woo Park, Jae-Hyung Wi, Won Seok Han, Jeha Kim, Mann-Ho Cho, Dongseop Kim, and Yong-Duck Chung: Non-toxically enhanced sulfur reaction for formation of chalcogenide thin films using a thermal cracker. Journal of Materials Chemistry A. 2014; **2**: 14593–14599. DOI: 10.1039/c4ta02507e

[43] Jae-Hyung Wi, Tae Gun Kim, Jeong Won Kim, Woo-Jung Lee, Dae-Hyung Cho, Won Seok Han, and Yong-Duck Chung: Photovoltaic performance and interface behaviors of Cu(In,Ga)Se_2 solar cells with a sputtered-Zn(O,S) buffer layer by high-temperature annealing. ACS Applied Materials & Interfaces. 2015; **7**: 17425–17432. DOI: 10.1021/acsami.5b04815

[44] Dae-Hyung Cho, Woo-Jung Lee, Jae-Hyung Wi, Won Seok Han, Tae Gun Kim, Jeong Won Kim, and Yong-Duck Chung: Interface analysis of Cu(In,Ga)Se_2 and ZnS formed using sulfur thermal cracker. ETRI Journal. 2016; **38**: 265–271. DOI: 10.4218/etrij.16.2515.0031

[45] Woo-Jung Lee, Hye-Jung Yu, Jae-Hyung Wi, Dae-Hyung Cho, Won Seok Han, Jisu Yoo, Yeonjin Yi, Jung-Hoon Song, and Yong-Duck Chung: Behavior of photocarriers in the light-induced metastable state in the p-n heterojunction of a Cu(In,Ga)Se_2 solar cell with CBD-ZnS buffer layer. ACS Applied Materials & Interfaces. 2016; **8:** 22151–22158. DOI: 10.1021/acsami.6b05005

http://dx.doi.org/10.5772/66350

[46] Tokio Nakada, Tomoyuki Kume, Takahiro Mise, and Akio Kunioka: Superstrate-type Cu(In,Ga)Se_2 thin film solar cells with ZnO buffer layers. Japanese Journal of Applied Physics. 1998; **37**: L499.

[47] Chang-Soo Lee, Suncheul Kim, Essam A Al-Ammar, HyuckSang Kwon, and Byung Tae Ahn: Effects of Zn diffusion from (Zn,Mg)O buffer to CIGS film on the performance of Cd-Free Cu(In,Ga)Se_2 solar cells. ECS Journal of Solid State Science and Technology. 2014; **3**: Q99–Q103. DOI: 10.1149/2.003406jss